X-RA Y SPECTRAL EVOLUTION OF

THE CRAB PULSE

Steven H. Pravdo[1,2,3]

Lorella Angelini [3,4]

and

Alice K. Harding[5]

submitted to the *Astrophysical* ***Journal*** April 28, 1997

'The research described in this paper was carried out in part by the Jet Propulsion Laboratory, California Institute of Technology, under contract with the National Aeronautics and Space Administration.

[2]Jet Propulsion Laboratory, Mail Stop 306-431, California Institute of Technology, Pasadena, CA 91109. email: spravdo@ccmail.jpl.nasa.gov

[3]*RXTE* guest investigator

[4]University Space Research Association, Laboratory for High Energy Astrophysics, NASA/Goddard Space Flight Center, Code 668, Greenbelt, MD 20771. email: angelini@lheavx.gsfc.nasa.gov

[5]Laboratory for High Energy Astrophysics, NASA/Goddard Space Flight Center, Greenbett. MD 20771. email: harding@twinkie.gsfc.nasa.gov

ABSTRACT

The Crab Pulsar was observed with the X-ray detectors on the Rossi X-ray Timing Explorer (*RXTE*) on May 2, 1996. The large area, high time resolution, extended energy range, and moderate energy resolution of the *RXTE* instruments provided an unprecedented measurement of the Crab pulsar spectrum as it evolved in phase across the 33 msec pulse. The X-rays are pulsed over the detected range 5-200 keV, and the pulse shape changes with energy in concert with the spectral evolution. The X-ray pulse as seen with RXTE has a well-known double-peak shape with significant emission in the smaller phase region between the peaks (the "interpeak") and no detectable pulsed emission in the "nebular" phase region. The new *RXTE* results show an evolution of the spectral index across the pulse in a "reverse S-shape": (1) the spectrum softens (i.e. the power-law index increases) starting at the leading edge of the first peak until the intensity maximum of the first peak; (2) hardens in the interpeak region; and (3) softens throughout the second peak, The temporal resolution and statistical quality of prior data did not allow behaviors (1) nor (3) to be seen, while behavior (2) confirms previous results, but with higher temporal and spectral resolution. Thus there is a significant difference of the spectral evolution across each of the two intensity peaks. While existing models can, in principle, explain spectral behaviors (2) and (3), the hardening towards the leading edge of the first peak (behavior 1) is unexpected. This hardening occurs in the same phase region where at much lower energies there is enhanced emission in a "precursor" to the first radio peak, and at much higher energies there is a possible broadening of the first y-ray peak. The discovery that the first X-ray peak is symmetric with respect to spectral evolution is a new clue toward

understanding the interaction between emerging photons and the magnetic field which creates the pulse and defines its phases.

Subject headings: pulsars: individual (Crab) --X-rays: pulsars

1. INTRODUCTION

The beloved Crab Pulsar is the prototype and best studied of the isolated pulsars. It is the neutron star remnant of the supernova explosion which created the Crab Nebula, and is still located within the Nebula. Since its discovery (Staelin & Reifenstein 1968), the Crab has been shown to pulse in a wide energy range from radio to gamma ray (Thompson et al. 1977). The pulse maintains a two peaked shape over this large energy range and there is no large phase delay between the peaks when comparing the pulse in different bands. However, the details of the pulse shape change with energy (e.g. Eikenberry & Fazio 1997), or fundamentally, the spectrum evolves with pulse phase. The pulse itself is a manifestation of an asymmetry introduced into the emission by the superstrong (-10^{12} gauss) pulsar magnetic field; the pulse phase represents different angles with respect to the magnetic field direction. The spectrum at each phase thus consists of photons preferentially emitted at that angle or scattered into that angle. The simplest form and starting point of the emission asymmetry is that the magnetic field creates a magnetic polar cap or caps on the neutron star surface. These produce enhanced emission as the stellar rotation sweeps them across the field of view.

Where are the X-rays generated in the pulsar environment and how do they finally emerge to the observer? The phase-resolved spectroscopy discussed in this paper may gives clues toward the resolution of these questions. The “intensity” pulse, is formed in part by energy-independent processes ranging from simple geometry to general relativity (Ftaclas, Kearney, & Pechenick 1986). But the “spectral” pulse which we will describe, must arise from the energy-dependent processes near the pulsar.

The goal of this *RXTE* experiment was to perform pulse phase spectroscopy of the Crab pulsar at higher temporal resolution and statistical accuracy than had been possible before ($2.3). In addition, the extended energy range of *RXTE* allowed study of the pulse spectra over a broad band ($2.4). Finally, current models for high-energy pulsar emission are confronted with these results (53.3).

2. OBSERVATIONS, ANALYSIS, and RESULTS

2.1 *Detectors and Observing Modes*

The Crab was observed on May 2, 1996 with the *RXTE* instrument suite (Bradt, Rothschild, & Swank 1993). The extent of the observation was 14.5 ks but the effective times were significantly reduced by operational effects such as satellite passage through the South Atlantic Anomaly radiation belt. Data were obtained from two sets of detectors: (1) PCA consisting of 5 Proportional Counter Arrays and (2) HEXTE consisting of 2 clusters of four NaI(Tl)/CsI(Na) phoswich scintillation counters. All the PCA detectors were operating as were the 8 HEXTE counters, although one of the latter did not provide spectral information. The PCA and HEXTE energy ranges were 5-60, and 16-250 keV, respectively. The low-energy PCA cutoff was chosen to be 3 keV to mitigate against data saturation but an in-orbit gain change caused the cutoff to be closer to 5 keV. Observing times of the PCA and HEXTE detectors substantially overlapped but were not identical since the detectors have different operational modes. In particular, HEXTE rocks between on- and off-source positions

leading to a reduction of on-source time by >50%. The fields-of-view of these non-imaging detectors contained both the Crab Pulsar and the Crab Nebula.

The flexibility of the *RXTE* data system features spectral and timing modes which enable this pulsar-phase-resolved spectroscopic observation. In addition to standard data and a count rate monitor, the PCA data were also obtained in an "event mode" which provided pulse-height analyzed (PHA) data in 128 channels with 250-μsec time resolution. These data were kept in an on-board buffer which was read out every 8 seconds in the first and last third of this observation, and every 1 second in the middle third. Because of dead-time and rate considerations, only the middle third of the PCA data were used in the analysis. The net time for these PCA data was 2880 s.

HEXTE data was obtained in an event mode which had 2 millisecond time resolution. All the HEXTE data were used in the analysis. The net time for the HEXTE data was 2133 s.

2.2 *Pulse Period and* **Shape**

The Crab Pulsar period was determined by folding the 250 μsec-PCA data over candidate periods after time-of-flight and barycentric corrections. The accuracy of the period determination is consistent with a phase shift of less than 1°/0 over the 2880-s interval. This ensures that there is minimal mixing of photons from one of the hundred PCA spectral phase bins described below to adjacent bins. Figure 1 shows the pulse light curve obtained from these data. The familiar double peak shape is evident, with a stronger first peak and interpeak emission, The period is 33.4565 16+ 0.000004 msec. This value is consistent with the interpolated radio pulse period of 33.456513 msec (Nice 1997). The same period and period accuracy were required for the HEXTE data which

spanned 14520 s but were only folded into 25 phase bins. Evidence of pulsation is present up to -200 keV. The higher energy pulse (Figure 2) shows that the second peak becomes more intense than the first peak and the interpeak increases (e.g. Ulmer et al. 1994).

The pulse phase was determined by fitting models to the profile of the first peak with the 250-μsec PCA data. A Lorentzian fits the peak better than a Gaussian but the centers (≡ phase zero) agree to 0.001 phase. The pulse width is 0.023 phase, and is symmetric in intensity with deviations $\lesssim 0.03$ from the Lorentzian model. A comparison of the absolute pulse phase of several *RXTE* observations (including this one) versus the radio pulse yields offsets on the order 0.5 ms (Rots 1997) somewhat larger than the upper limit of 0.3 ms reported by Ulmer et al. (1994). A precursor to the first peak in the 300-400 MHZ radio (e.g. Moffit & Hankins 1996) occurs near -0.05 phase, as does a possible broadening in the y-ray peak (Fierro 1995).

2.3 ***High Time Resolution Pulse Phase Spectroscopy***

High time resolution pulse phase spectroscopy was performed with the 250-μsec PCA event data. The PCA data were folded over the pulse period into 100 phase bins. A background spectrum was-obtained from the flat phase region, phase 0.55-0.85, the "nebular background" (NB). This NB spectrum was used to subtract phase-independent Crab Nebula X-rays, as well as the cosmic and internal backgrounds from each of the remaining pulsar phase bins.[6]

---

[6]To the extent that "pulsar" emission is negligible in this phase region, this is a valid procedure. A measurement using lunar occultations of the pulsar in the 1-20 keV range (Wolff et

Spectral analysis of 60 pulsar phase bins (phase 0.9-0.5) was performed using an epoch-appropriate detector spectral response matrix, the NB background, the program XSPEC, and a simple power-law model, dN/dE (photons cm^{-2} S-l keV^{-1}) = $CE^{-\alpha}$, where C is the normalization and ***a*** is the power-law index. The results are shown in Table 1 and Figure 1. There is a clear and significant change of ***a*** with pulse phase, which has a distinct "reverse-S" shape. This index change does not follow the intensity profile. The spectrum softens from the leading edge of the first peak to the first peak maximum, hardens through the interpeak, and softens again through the second peak. The spectral hardening toward the leading edge of the first peak occurs in the same phase region where the radio precursor pulse occurs (e.g. Moffett & Hankins 1996) and where the first y-ray peak may asymmetrically broaden (Fierro 1995). The χ^2_{dof} (χ^2 per degree of freedom) of the power-law fits is usually acceptable but rises to 1.4 in a couple of phase bins distributed over the pulse. Figure 3 illustrates the two extreme inferred incident spectra, both from 0.01 phase bins. The softest spectrum

---

al. 1975) found an upper limit of about 3°/0 to the pulsar-to-nebula intensity ratio. This estimate can not be applied exactly to the *RXTE* case because the ratio is spectrally and thus detector dependent. The pulsar contribution to the total X-rays increases from 2-20% over the *RXTE* energy band (e.g. Toor & Seward 1977) so this upper limit would be higher for HEXTE data than for PCA data. Nevertheless, even with some pulsed emission in this region (e.g. Harnden & Seward 1984 reported significant 0.1-4.5 keV pulsed emission in this phase interval but did not estimate its intensity), this is the best constant background for pulse phase spectroscopy. Most importantly for this study, ***relative*** spectral changes are not affected. Another piece of evidence for the lack of a significant pulsed component in the NB is that the nebular phase region is fit well by a constant intensity vs. phase model.

(upper) is from the maximum of the first peak, phase 0.0025 with α = 1.97, and the hardest (lower) is from phase 0.2125 with α = 1.58. The best-fit models (solid lines) are also shown, As discussed below (§3 .3) if these differing spectral indices were maintained to higher energies the two spectra would cross at -2.8 MeV.

2.4 *Broad Band Pulse Phase Spectroscopy*

Broad-band spectral analysis was performed simultaneously with PCA and HEXTE data by using XSPEC on 16 pulsar phase bins containing both PCA and HEXTE data in the range 5-250 keV. The HEXTE data have lower temporal resolution, 2 ms, than the PCA data. To combine these data in pulse phase spectroscopy, the PCA temporal resolution was degraded to match HEXTE. Even if the HEXTE data had the same temporal resolution, the HEXTE count rate would have been too low to get good statistical accuracy in 100 phase bins. Therefore, PCA and HEXTE data were each binned into 25 pulse phase bins, with 128 and 256 PHA channels, respectively. In practice the HEXTE spectral data $\geq$ 150 keV were too noisy to be useful. A HEXTE NB spectrum was also accumulated from the 0.55-0.85 phase region. The relative normalization between the PCA and HEXTE data was initially left as a free parameter for all the spectra,

An instrumental problem in these data wherein the PCA and HEXTE pulses were out of phase with respect to each other by less than one phase bin, was solved by empirically shifting the pulses until the overlap energy range from 16-50 keV was consistent between the two detector sets. This phase shift was also confirmed by the fact that before the shift the combined spectral fits showed a variation in the relative normalizations between the two detectors by a factor of 3.5, from 0.4-1.4,

for the 16 pulsar phase bins. The maximum variations were correlated with large pulse intensity derivatives, just where an inter-detector phase shift would be most critical. After this empirical phase shift (by 0.27 msec in the sense that the HEXTE phase was later than the PCA phase) the variation in the relative normalizations with pulse phase decreased substantially to 0.74 ± 0.08. The fact that the average relative normalization of HEXTE to PCA is 0.74 indicates that the estimate of the HEXTE area is high relative to the PCA, or equivalently the PCA estimate is low relative to HEXTE. (See $2.5 for another, consistent estimate of this relative normalization, and Appendix A,)

There is now no reason to accept one detector's normalization over the other's. If we divide the effect of the normalization error equally between the two detectors, the average area uncertainties are 15°/0 per detector. This eliminates any apparent discontinuities in the spectra and provides consistency in the 16-50 keV overlap region. Further improvement in the determination of the normalization awaits definitive calibrations. Previous observations with different detectors also do not help resolve the issue (see $3.2 and $3.4).

Figure 4 shows the evolution of the power-law index with pulse phase as in Figure 1 but with the simultaneous PCA and HEXTE data at lower temporal resolution. Note that the error bars have decreased in each phase bin because there are four times more PCA data per bin. However, the goodness of the fits have also decreased (see below). Figure 4 also shows that the form of the result is independent of the exact value for the relative normalization, An increase in the normalization moves the indices up in parameter space but does not affect the shape of the reverse-S evolutionary curve. The HEXTE data alone are consistent with this spectral behavior but do not have sufficient temporal resolution to show the hardening in the first peak leading edge (Figure 5). Only the first 14 pulse phase spectral results are shown since the final two bins have very low net counts and the

spectral indices are poorly determined. The pulse phase spectral evolution is thus seen in two detectors separately and combined, and has the same character independent of the exact value of the relative normalization between the two detectors.

The fits become worse when the PCA temporal resolution is degraded to match that of HEXTE (Figure 6). The χ^2_{dof} at the peak of the pulse is now 3.3 for the PCA data alone. A better fit is obtained, χ^2_{dof} = 2.1, when a more complex broken- or two-power-law model is used (Figure 6). It is hard to place too much physical significance on the model with more parameters since the data being fit consist of spectra with different power-law indices, a fact extracted from the analysis of the data with higher temporal resolution ($2.3).

2.5 *Crab Nebula Spectrum*

The broad-band NB spectrum was analyzed for a separate determination of the relative HEXTE to PCA normalization and to compare *RXTE* to prior measurements. The NB spectra, as described above, are extracted from the 0.55-0.85 phase region. However, in this case, the comparison of data from the different detectors depends very weakly upon any relative pulse phase shift since the data come from constant intensity phase regions. The result for the average relative normalization was 0.72 for the two HEXTE clusters relative to the PCA, consistent with the pulsar result.

The best-fit power-law model for the Nebula spectrum subtracting off-source background is shown in Table 2. Because the photon noise is so low (= high count rate) these data reveal the remaining uncertainties in the detector response matrices and the fit does not yield an acceptable χ^2.

However, the ratios of model-to-data in each PHA channel do not deviate by more than -1 % from unity. The model has the form $dN/dE = (8.3+1.2)\ E^{-2.1}$, where the spectral index uncertainty is less than 1% and the normalization uncertainty is dominated by detector effective area unknowns (§2.4). Fortunately this imprecision does not affect the described pulse-phase spectroscopy since the source and background spectra come from the same detectors.

3. DISCUSSION

3.1 Evolution of the Pulsar X-ray Spectrum

In an early X-ray result at low-resolution, Toor & Seward (1977) showed that the pulsar spectrum was softest in the first peak, hardest in the interpeak, and had an intermediate value in the second peak. At higher temporal resolution, Pravdo & Serlemitsos (1981) traced this spectral evolution in 10 pulse phase bins. Their Figure 1 shows an effect entirely consistent with the *RXTE* result but without the temporal resolution or statistical quality to detect the hardening of the spectrum toward the leading edge of the first peak. Now, the *RXTE* data, and in particular, the highest temporal resolution PCA data show further details. In the first peak, the spectral index change appears to be linked, rising and falling, with the pulse intensity changes, but in the second peak the link is gone. This indicates that the peaks are not physically symmetric: e.g., they do not arise from two similar polar caps, or from the leading and trailing edges of a single, symmetric emission region. The well-known intensity asymmetry between the two peaks could be caused in an energy-independent process (e.g. Compton scattering in a low magnetic field) separate from the emission region. But only

energy- and angle-dependent processes near the emission regions could give rise to and maintain the observed, ordered spectral changes.

3.2 *Spectral* **Evolution** *at* **Other** *Wavelengths*

Spectral evolution occurs in other wavelengths. In the IR-visible-UV a number of observers have found that the interpeak region is harder (bluer) than the main peak (Muncaster & Cocke 1972, Groth 1975, Eikenberry et al, 1996)

For the higher energy y-ray data, pulse phase variability is seen when the statistics allow. Table 2 shows the model results of the averaged RXTE spectra for the first peak, interpeak, and second peak, where the RXTE data are binned into *CGRO*-defined phase bins (Ulmer et al. 1995). The *CGRO* models (Ulmer et al. 1995) match the *RXTE* data best near 100 keV but the extrapolations to lower energy all fall below the *RXTE* results by as much as a factor of -2. It is unclear whether this is a manifestation of the normalization uncertainty or whether the *CGRO* "broken power-law" models, which flatten the spectra in the *RXTE* regime, are inconsistent with the *RXTE* results. Ulmer et al. (1994) did not find significant evidence of pulse phase spectral variability in the 0. 1-1 MeV range. However, Fierro (1995) found that the *CGRO* EGRET data show a pulse phase spectral evolution at energies > 100 MeV similar to that reported herein for the X-ray data. These y-ray data show an increase and subsequent decrease in "hardness ratio" from the first through the second peak, There is no apparent hardening in the leading edge of the first y-ray peak, but there is insufficient temporal resolution or statistical quality to rule it out.

3.3 *Pulse Spectral Evolution Modeling*

The models of high-energy pulsar emission discussed below have focused their attention on the highest energy processes and attempted to explain the y-ray emission. This may be in part because these are easiest to explain, while placing the most stringent energetic requirement on the system, The hope that an extrapolation of the models will be made to X-ray energies has not yet been fulfilled. A further unified model which encompasses the radio and visible emission seems even farther from fruition. For the case of the Crab Pulsar two surprising observational facts have emerged which should guide the modeling: first, the pulses appear to be in phase over a broad energy range from 10^{-6} eV to 10^{8} eV (e.g. Moffit & Hankins 1996, Fierro 1995); and second, the variation of the phase-resolved spectrum as reported here in the 5-150 keV band, is surprisingly consistent with the evolution in some energy bands from 1 eV to >100 MeV ($3.2).

There is, however, an apparent contradiction in these two facts. Harder interpeak emission means that interpeak intensity increases relative to peak intensity. This is true, in part, as demonstrated by the growth of the interpeak emission and of the second peak relative to the first peak at >100 keV (Fig. 4). However, if this trend continued from the *RXTE* energy range, the interpeak emission would equal the first peak emission at -2.8 MeV. This value is derived by extrapolating the measured *RXTE* spectra, in particular from phases 0.0025 and 0.2125, Table 1 and Figure 3. In fact, Ulmer et al. (1994) found that the interpeak reaches a maximum, still below that of the peaks, near 1 MeV. Thus, the interpeak spectrum turns over. Then, at even higher energies >100 MeV, the trend of harder interpeak emission starts again (Fierro 1995). The combined spectral variations of the interpeak between 5 keV and 100 MeV require structure in the interpeak spectrum, possibly

implying an additional component or enhancement (see also Knight 1982, 1983). The hardening of the visible interpeak emission can also be included in this pattern since it again can not persist without contradicting the recovery of the pulse shape and phase several decades higher in energy. It is not now possible, but tempting, to explain these properties with a common emission mechanism.

In all these energy ranges, only the *RXTE* data have sufficient statistical accuracy to see the hardening in the leading edge of the first peak. The observed spectral variations measured with a resolution 0.01 of the pulsar phase constrain the size of the regions producing the emission, For the observed phase variations (and temporal variations) to not be smeared out by light travel time across the emission region, the radial dimension of the region must be smaller than 107 cm. This in itself argues against models in which the emission occurs more than 10 neutron star radii from the surface.

It is not yet clear how and where in the pulsar magnetosphere the high-energy radiation originates. Polar cap models (Daugherty & Harding 1996, Sturner & Dermer 1994) assume that particles are accelerated above the neutron star surface and that y-rays result from a curvature radiation or inverse Compton induced pair cascade in a strong magnetic field. In these models, hollow-cone emission from a single magnetic pole can produce the double-peaked profile, as well as the phase-resolved spectral variation observed in high energy y-rays wherein the interpeak emission is harder than the emission from the peaks. The radiation pattern is a hollow cone centered on the pole because the curvature radiation emissivity peaks at the polar cap rim, where the field line radius of curvature is smallest, and is zero at the magnetic pole, where the radius of curvature is infinite. The hardest emission is expected to occur near the pole - the interpeak region - where the emission is pure curvature radiation that is not softened by cascading. Near the polar cap rim, where the peak emission originates, the cascades are most extended, producing a softer spectrum. However, to

explain the new X-ray results, there must be an asymmetry between the leading and trailing edges of the rim emission to produce the asymmetric spectral behavior; i.e. the hardening in the leading edge of the first peak. The emission outside the rim, and outside the peaks in the pulse profile, comes from high-altitude curvature radiation from primary particles that have lost most of their energy and has the softest spectrum, Polar cap cascade model spectra in the X-ray band have not been fully explored, but the indication is that curvature radiation maybe relatively more important than synchrotrons in the X-rays. An additional emission mechanism, such as inverse Compton, may also be operating to produce the X-ray and lower energy emission in the Crab. However, if there is another mechanism it must create the same kind of hardening in the X-rays (and optical) interpeak region as occurs in the y-rays.

Outer-gap models (Cheng, Ho& Ruderman 1986; Romani 1996) may find it more difficult to explain the above constraints on radial size of the emission region since the radiation can in principal originate over distances that are a significant fraction of the light cylinder radius (- 10^8 cm). These models assume that acceleration occurs along null charge surfaces in the outer magnetosphere and that y-rays result from photon-photon pair production-induced cascades. They divide into two regimes: Crab-like, where curvature radiation photons interact with non-thermal X-ray emission from the gap-accelerated particles to produce pairs and a synchrotrons self-Compton spectrum; and Vela-like, where curvature radiation photons interact with thermal X-rays from the neutron star to produce pairs and a purely curvature radiation spectrum, Again, models have concentrated on the high energy y-ray data and the Vela-like outer gap radiation can produce the observed phase-resolved spectral variations of the Vela pulsar (Romani 1996). Although a model for the phase-averaged spectrum of the Crab pulsar (Ho 1989) gives a good fit to the observed spectrum, no phase-resolved

spectra have been computed (and would be a difficult task, given the highly non-linear nature of the Crab-like cascade).

The *RXTE* data by virtue of its unprecedented statistical quality and temporal resolution add a new phenomenon to the Crab inventory: the spectral hardening in the leading edge of the first peak. This spectral behavior further distinguishes the two peaks, already distinguished by different intensity behavior. The first X-ray peak appears symmetric in both the intensity and spectral domains while the second peak does not. The hardening in the leading edge can not be pursued to earlier phase because the pulsar photons are no longer detectable over the nebular background. But this maybe an accident of geometry. If we could measure the pulsar at earlier phase, then the symmetry of the first peak might be more easily modeled and understood. Pulse formation models must confront this new feature as well as the fourteen energy decades of pulse phase alignment, and the, at least, nine energy decades of recurrent pulse spectral hardening in the interpeak.

3.4 *The Crab Spectra as Calibration Sources*

For many years the Crab spectra - pulsar, nebula, and combined - have been used in X-ray spectroscopy for calibration (e.g. Nørgaard-Nielson et al. 1994) and in broad band comparisons (e.g. Ulmer et al. 1994, 1995). For the pulsar and combined spectrum these are dubious choices since it is clear that they are, in fact, hybrids of different spectra.

For the Crab Nebula, observers agree that the spectrum is well-fit with a power-law continuum from 5-100 keV. Indeed the *RXTE* data are of this form ($2.4). But there is a lack of agreement on the normalization of this spectrum. Curiously, proportional counter observations tend

toward higher normalizations by as much as 30°A compared to scintillators. Unfortunately, these *RXTE* data can not now resolve this issue, There continues to be a 25% difference in the normalization measured with the two sets of detectors, despite the simultaneity of the observation and the substantial energy range overlap from 16-50 keV. Proportional counter data (Toor & Seward 1977 and PCA) tend to lie above the scintillator data (Strickman, Johnson, & Kurfess 1979 and HEXTE). The exceptions to this rule are the proportional counter data of Pravdo & Serlemitsos (198 1) and the scintillator data of Jung (1989). This sorry state may not be resolved until another type of detector (e.g. CCD) weighs in with another answer.

We acknowledge the contributions of the PCA and HEXTE *RXTE* teams to this work including J. Lochner, D. Gruber, P. Blanco, A, Rots, and C. Day. SHP thanks D. Nice for helpful discussions of the Crab Pulsar radio ephemeris.

REFERENCES

Bradt, H. V.; Rothschild, R. E.; Swank, J. H., 1993, Astronomy and Astrophysics Supplement Series (ISSN 0365-0138), vol. 97, no. 1, p. 355-360

Cheng, K. S., Ho, C. & Ruderman, M. A. 1986, ApJ, 300, 500

Daugherty, J. K. & Harding, A. K. 1996, ApJ, 458, 278

Eikenberry, S. S. et al. 1996, ApJ, 467, L85

Eikenberry, S. S. & Fazio, G. G. 1997, ApJ, 476, 281

Fierro, J. M. 1995, Ph.D. Thesis, Stanford University

Ftaclas, C., Kearney, M. W., & Pechenick, K., 1986, ApJ, 300, 203

Groth, E. J. 1975, ApJ, 200,278

Harnden, F. R. & Seward, F. D. 1984, ApJ, 283, 279

Ho, C. 1989, ApJ, 342,396.

Jahoda, K. 1997, http: //lheawww.gsfc.nasa.gov/users/keith/deadtime/deadtime.html

Jung, G. V. 1989, ApJ, 338, 972

Knight, F. K. 1982, ApJ, 260, 538

Knight, F. K. 1983, in Positron-Electron Pairs in Astrophysics, ed. M. L. Burns, A. K, Harding,

Muncaster, G. W. & Cocke, W. J. 1972, ApJ, 178, L13

Nice, D. 1997, http: //pulsar. princeton.edu/

Nørgaard-Nielson, H. U., Budtz-Jørgensen, Westergaard, N. J., & Schnopper, H, W. 1994, A&A, 284, 705

Pravdo, S. H. & Serlemitsos, P. J. 1981, ApJ, 246,484

Romani, R. W. 1996, ApJ, 470,469.

Rots, A. 1997, private communication

Staelin, D. H. & Reifenstein, E. C. 1968, Science, 162, 1481

Strickman, M. S., Johnson, W. N., & Kurfess, J. D. 1979, ApJ , 230, L15.

Sturner, S. J. & Dermer, C. D. 1994, ApJ, 420, L79.

Thompson, D. J. et al. 1977, ApJ, 213, 25

Toor, A. & Seward, F. D. 1977, ApJ, 216, 560

Ulmer, M. P., et al. 1994, ApJ, 432,228

Ulmer, M. P. et al. 1995, ApJ, 448, 356

Wolff, R. S. et al. 1975, ApJ ,202, L77

FIGURE CAPTIONS

1. The Crab Pulse, 5-60 keV, measured with 250-μsec PCA data (solid line and filled diamonds), power-law index with pulse phase (crosses), and reduced χ^2 (open circles) for each bin. 60 pulse phase bins are spectrally analyzed; the other 40 bins are either nebular background or transition bins with too few net counts for useful spectroscopy.

2. HEXTE data, 100-250 keV, folded over the Crab pulse period.

3. Two extreme inferred incident spectra, upper from phase 0.0025 near the first peak maximum, and the lower from phase 0.2125 in the interpeak, and the best-fit models (solid lines).

4. Pulse phase spectroscopy of 16 phase bins combined PCA and HEXTE data. The power-law indices are shown for two assumed values of the relative normalization between the two detector types. The other 9 phase bins are either nebular background or transition bins with too few net counts for useful spectroscopy.

5. Pulse phase spectroscopy of 14 bins of HEXTE data: pulse profile and power law indices. The other 11 phase bins are either nebular background or transition bins with too few net counts for useful spectroscopy.

6. $\chi^2_{d.o.f.}$ for the PCA data in 16 phase bins for single and broken power-law models. The other 9 phase bins are either nebular background or transition bins with too few net counts for useful spectroscopy.

APPENDIX A.

Deadtime and Detector Normalization Issues

Dead time occurs in high count rate sources because the instrument fails to process a count received from the source in time to process the next count. In this definition, dead time can occur throughout the detection and data storage systems. An increasing fraction of the counts is lost as the count rate increases. Since this paper is primarily a spectral investigation, dead time effects are not important as long as they are spectrally independent. This is the case according to the best information from the *RXTE* instrument teams.

The dead time in the PCA data depends critically on the time in which the PHA buffer is read out. The maximum number of counts held in this buffer is 16384. Since the Crab count rate averaged -8000 counts/sec, as expected, the buffer was saturated in the 8-s mode, and the dead time was large.

These 8-s data are usable for spectral analysis, in principle, since the dead time is spectrally independent. The 1-s data had a negligible dead time even at the pulse peak of 12000 counts/see. Since these data not only had a negligible dead time, but also provided 4 times as many counts as the combined 8-s data, we have chosen at this time to analyze only the 1-s PCA data. The other source of dead time in these data is the time to pulse-height analyze an event. For the PCA this time is approximately 10 μs per event (Jahoda 1997). The PCA dead time is pulse phase-dependent with a maximum at the main pulse peak of 2. 1°/0, and a minimum of 1. 10/0 in the "nebular" region. This variation is smaller than other systematic errors and is accounted for in the relative normalization between the PCA and HEXTE detectors in the spectral fitting,

HEXTE dead time is due primarily to non-source counts and is thus phase-independent. During this observation the HEXTE dead time was about 35%.

Extreme accuracy in the determination of the absolute normalization of the Crab flux is not critical for this investigation, again, because of the spectral focus. However, simultaneous spectroscopy with both detectors sets requires a determination of the relative normalization between the detectors, PCA and HEXTE. Detector dead times enter into this determination, Detector effective areas are known to some accuracy before launch, and in many cases on-orbit sources are used for a final calibration, Ironically the Crab is often used as a calibration. If both PCA and HEXTE areas are known to 15% then the relative normalization, which identically equals one if both are precisely known, could be from 0.74 to 1.35. In our combined spectral fits of different phase bins we have allowed the relative normalizations to be free parameters, This proved to be a good diagnostic of the relative timing between the two sets of detectors ($2.4).

Table 1. High Temporal Resolution Pulse Phase Spectroscopy Results

Pulse Phase	Normalization	Norm Error	Power-Law index a	Index Error	$X^2_{d.o.f.}$
-0.0975	0.089	0.039	1.67	0.15s	1.2
-0.0875	0.177	0.059	1.84	0.124	1.1
-0.0775	0.247	0.057	1.82	0.085	0.8
-0.0675	0.335	0.057	1.81	0.062	1.2
-0.0575	0.557	0.072	1.90	0.048	1.1
-0.0475	0.796	0.077	1,92	0.036	1.0
-0.0375	0.975	0.070	1.87	0.027	0.9
-0.027S	1.353	0.075	1.89	0.021	1.1
-0.0175	1.978	0.084	1.92	0.016	0.9
-0.0075	3.012	0.097	1.96	0.012	1.0
0.0025	4.308	0.106	1.97	0.009	1.2
0,0125	4.805	0.105	1.%	0.008	1.2
0.0225	3.225	0,093	1.94	0.011	1.0
0.0325	1.864	0.080	1.91	0.016	1.1
0.0425	1.143	0.068	1.85	0.022	0.9
0.0525	0.771	0.058	1.80	0.028	1.0
0.0625	0.510	0.048	1.72	0.034	0.9
0,0725	0.438	0.048	1.73	0.039	1.1
0.0825	0.444	0.056	1.80	0.046	0.7
0.0925	0.335	0.047	1.72	0.050	1.1
0.1025	0.250	0.038	1.63	0.053	1.1
0.1125	0.246	0.041	1.67	0.059	1.2
0.1225	0.274	0.048	1.73	0.063	1.0
0.1325	0.217	0.040	1.66	0.066	1.1

Table 1 Con't

0.1425	0.204	0.037	1.63	0.064	1.2
0.1525	0.269	0,053	1.78	0.072	1.0
0.1625	0.190	0.036	1.61	0.066	1.0
0.1725	0.226	0.041	1.68	0.066	1.1
0.1825	0.210	0.039	1.65	0.066	1.0
0.1925	0.197	0.037	1.63	0.066	1.1
0.2025	0.225	0.040	1.66	0,063	1.0
0.2125	0.195	0.033	1.58	0.059	0.9
0.2225	0.206	0.033	1.58	0.056	1.3
0.2325	0.253	0.038	1.64	0.053	0.9
0.2425	0.251	0.036	1.61	0.050	1.1
0.2525	0.273	0.037	1.62	0.047	0.9
0.2625	0.334	0.040	1.66	0.043	1.0
0.2725	0.413	0.046	1.71	0.040	1.1
0.2825	0.433	0.046	1.70	0.038	1.2
0.2925	0.445	0.042	1.67	0.033	1.4
0.3025	0.554	0.048	1.72	0.031	1.0
0.3125	0.590	0.047	1.71	0.029	0.9
0.3225	0.616	0.045	1.69	0.026	0.9
0.3325	0.732	0.048	1.71	0.024	0.9
0.3425	0.866	0.050	1.73	0.021	0.9
0.3525	1.088	0.057	1.77	0.019	1.1
0.3625	1.223	0.058	1.78	0.017	1.2
0.3725	1.417	0.060	1.79	0.016	1.2
0,3825	1.617	0.062	1.78	0.014	0.9
0.3925	1.911	0.06s	1.80	0.012	1.0
0.4025	2.213	0.068	1.81	0.011	1.3
0.4125	2.227	0.06s	1.79	0.011	0.9

Table 1 Cont

0.422S	2.083	0.070	1.83	0,012	1.4
0.4325	1.499	0.070	1.85	0.017	1.1
0.4425	1,135	0.075	1.90	0.025	1.1
0.4525	0.822	0.077	1.92	0.035	1.1
0.4625	0.640	0.080	1.94	0.047	0.9
0.4725	0.700	0.114	2.10	0,063	1.0
0.4825	0.333	0.071	1.90	0.080	1.2
0.4925	0.507	0.139	2.19	0,109	1.0
0.5025	0.208	0.078	1.94	0.141	1.1

Table 2. Broad-band, Phase-Averaged Spectra of Crab Pulsar and Nebula

Spectrum	Phase Region	Normalization	Norm Error	Power-law Index[a]	Index Error	$\chi^2_{d.o.f.}$
Peak 1	-0.15-0.05	2.175	0.027	1.92	0.005	1.6
Interpeak	0.08-0.27	0.286	0.011	1.69	0.013	1.0
Peak 2	0.30-0.44	1.331	0.017	1.80	0.005	2.2
Nebula	**0.55-0.85**	**8.295**	**0.026**	**2.14**	0.001	**2.5**

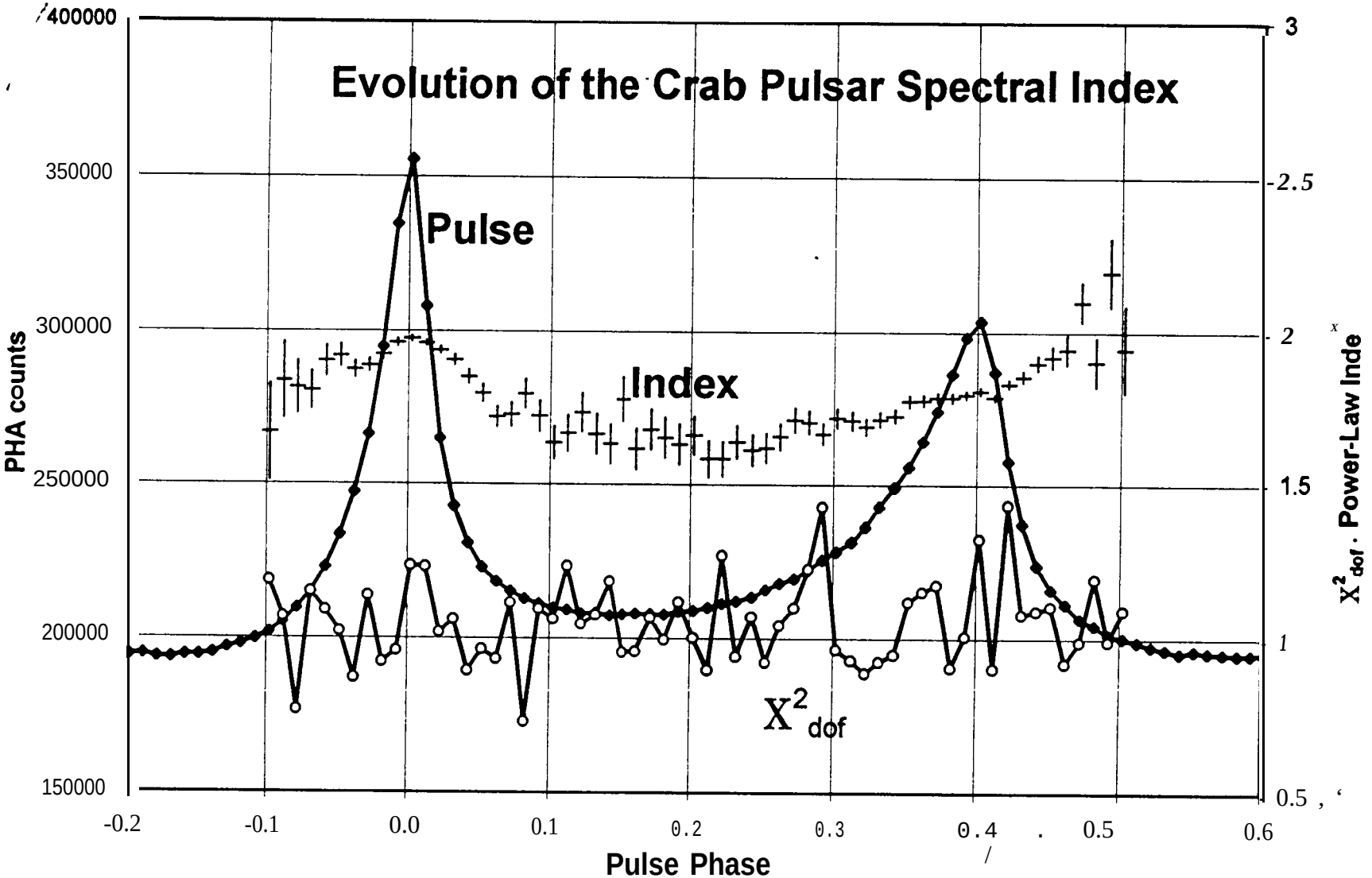
Evolution of the Crab Pulsar Spectral Index
Pulse
Index
X^2_{dof}
PHA counts
400000
350000
300000
250000
200000
150000
-0.2
-0.1
0.0
0.1
0.2
0.3
0.4
0.5
0.6
Pulse Phase
3
2.5
2
1.5
1
0.5
X^2_{dof} . Power-Law Inde

FIG. 1

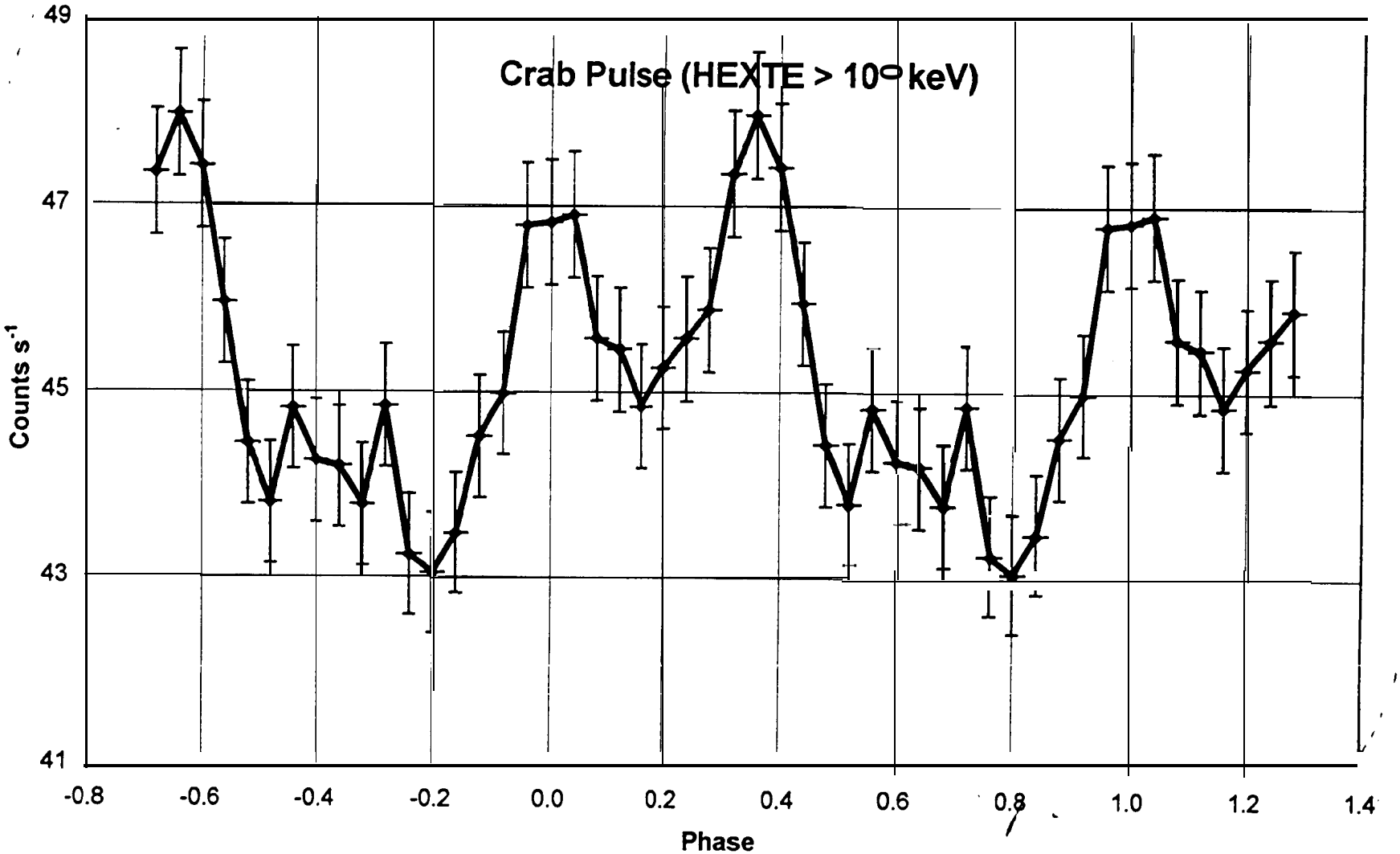
Crab Pulse (HEXTE > 10° keV)
Counts s-1
49
47
45
43
41
-0.8
-0.6
-0.4
-0.2
0.0
0.2
0.4
0.6
0.8
1.0
1.2
1.4
Phase

FIG 2

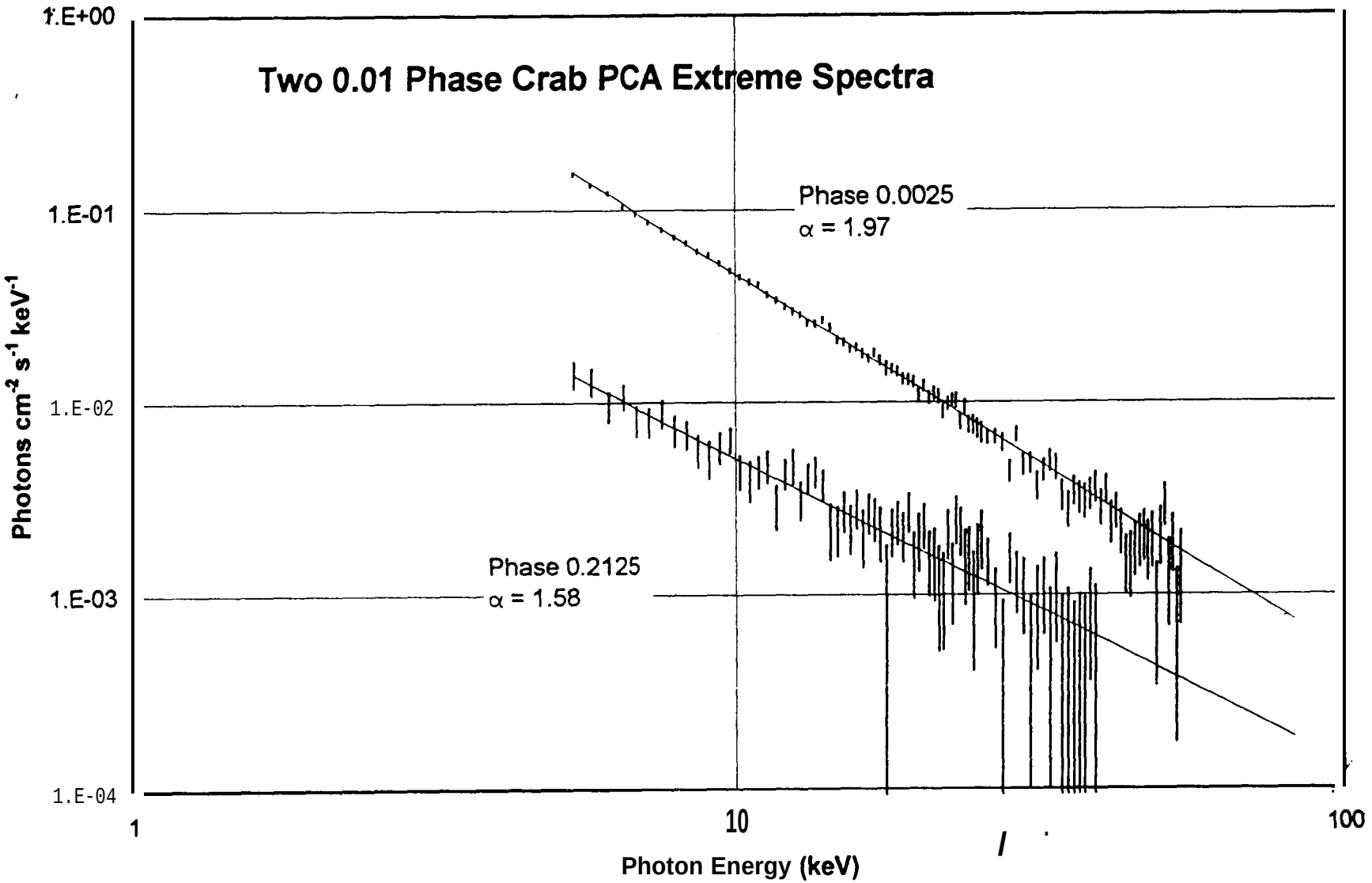
Two 0.01 Phase Crab PCA Extreme Spectra
Phase 0.0025
α = 1.97
Phase 0.2125
α = 1.58
1.E+00
1.E-01
1.E-02
1.E-03
1.E-04
Photons cm-2 s-1 keV-1
1
10
100
Photon Energy (keV)

FIG. 3

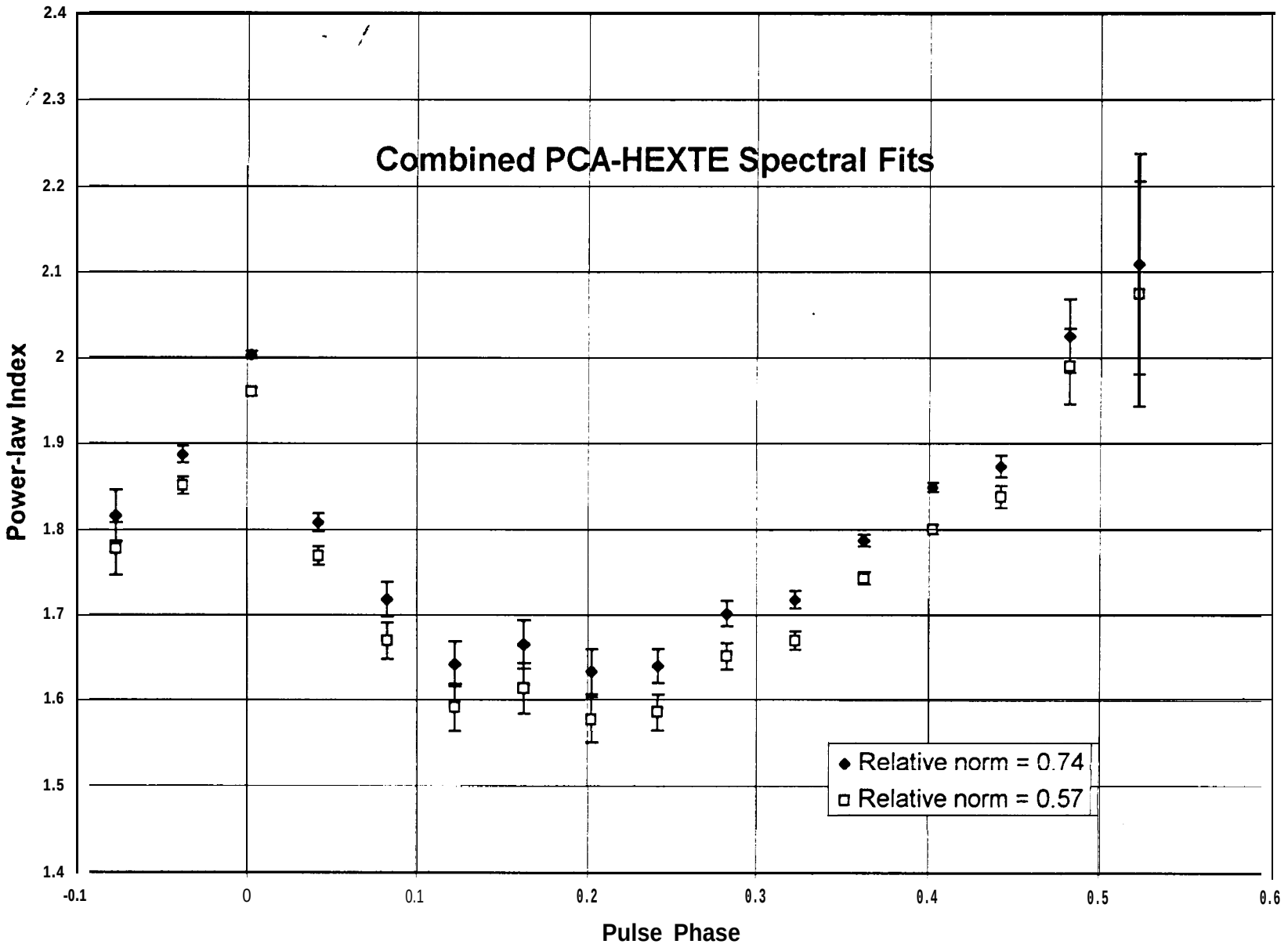
Combined PCA-HEXTE Spectral Fits
Power-law Index
Pulse Phase
2.4
2.3
2.2
2.1
2
1.9
1.8
1.7
1.6
1.5
1.4
-0.1
0
0.1
0.2
0.3
0.4
0.5
0.6
Relative norm = 0.74
Relative norm = 0.57

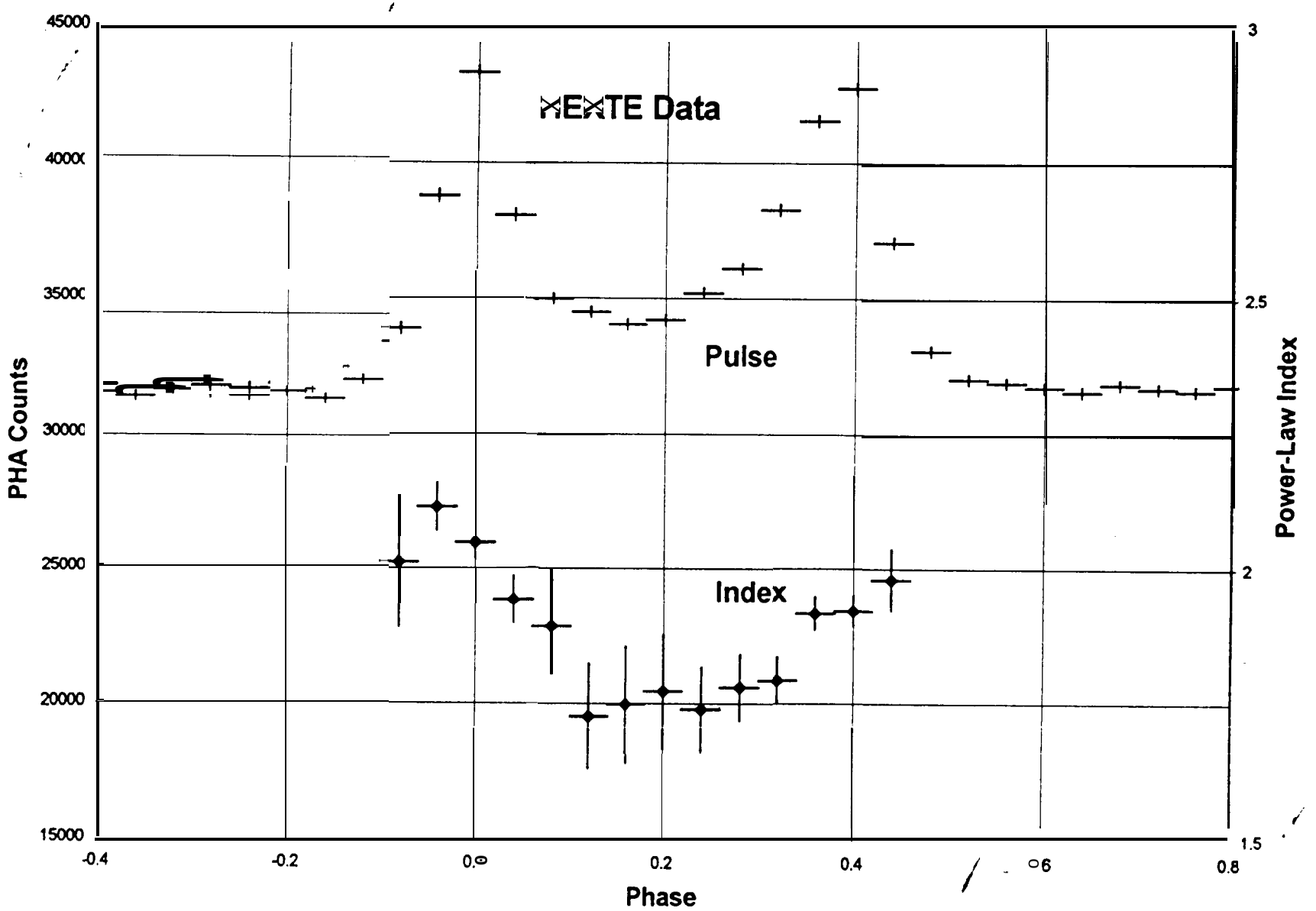
HEXTE Data
Pulse
Index
PHA Counts
Power-Law Index
Phase
45000
40000
35000
30000
25000
20000
15000
3
2.5
2
1.5
-0.4
-0.2
0.0
0.2
0.4
0.6
0.8

FIG. 5

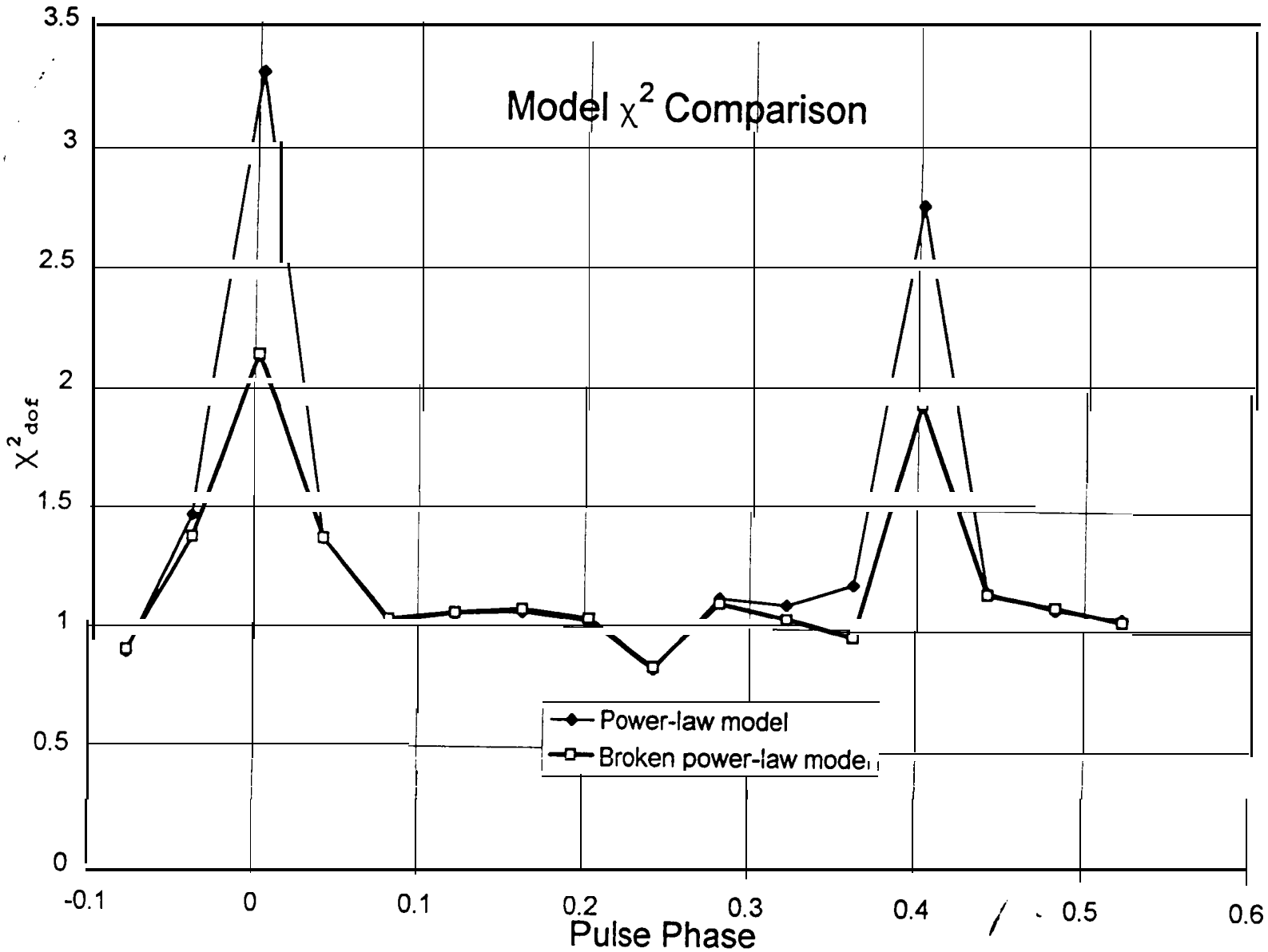
Model χ² Comparison
3.5
3
2.5
2
1.5
1
0.5
0
χ²dof
-0.1
0
0.1
0.2
0.3
0.4
0.5
0.6
Pulse Phase
Power-law model
Broken power-law model